Mechatronics 22 (2012) 481–490

Contents lists available at SciVerse ScienceDirect

Mechatronics

journal homepage: www.elsevier.com/locate/mechatronics

Passivity based visual servoing of mobile robots with dynamics compensation

Beatriz Morales [a], Flavio Roberti [a,b], Juan Marcos Toibero [a,b,*], Ricardo Carelli [a,b]

[a] Instituto de Automática (INAUT), Universidad Nacional de San Juan, Argentina
[b] Consejo Nacional de Investigaciones científicas y Técnicas (CONICET), Argentina

ARTICLE INFO

Article history:
Available online 4 October 2011

Keywords:
Visual servoing
Passivity
Mobile robots

ABSTRACT

This paper presents an image-based dynamic visual servoing to make a mobile robot able to track a moving object on the workspace by using a calibrated on board vision system. The stability of the proposed system is proved based on its passivity properties. A robustness analysis and an L_2-gain performance analysis are also presented. Experimental results are shown to illustrate the system performance.

1. Introduction

Mobile robots are mechanical devices which are able to navigate in a workspace with some degree of autonomy. Autonomous navigation is associated to the ability of obtaining information from the environment through external sensors, such as vision systems, range finders, or proximity sensors. Nowadays, the research in mobile robots control is focused on adding external sensors which, combined with advanced control strategies, allow the robot to perform different tasks in unknown environments or semi-structured ones, increasing their field of applications. Although range finders, which allow the robot to detect unknown obstacles or nearby walls, are the most common sensors, vision systems are widely used nowadays due to the quantity and quality of information that can be obtained from captured images.

According with the taxonomy proposed in [33], servo-visual control systems can be classified in: image-based visual servoing [4,19], when control errors are defined on the image plane; or position-based visual servoing [3], when the control errors are defined on the 3D Cartesian space. Additionally, the vision system can be considered *on board* [3,19,20,29], when it is placed on the mobile robot; different from the situation where the camera is fixed in the work space [4,5,26]. As regards the designed control law, visual control systems can be classified in: kinematics-based when only the kinematic models of the robot and the vision system are included in the control law development [19,20,29]; or dynamics-based when the robot dynamic model is taken into account in the controller design [4,5]. Although kinematics-based controllers usually have an acceptable performance, the robot dynamics should be included to reach better performance in tasks requiring high speed motions or heavy loads transportation.

Amid most relevant works related to autonomous navigation of mobile robots using visual information, [26] presents an image based control algorithm solving the point stabilization problem with a fixed camera. In [5], an image based algorithm for trajectory tracking is proposed considering also a fixed camera. In [3] an on board camera is used to obtain perspective lines in a corridor and a position based control algorithm is developed using this information to guide the robot along the corridor. Closer to our work, [19] uses an on board camera to allow the robot reaching a final position using two-view geometry. The same problem is solved using trifocal tensors in [20]. Additionally, vision based controllers have been developed for multi-robot systems, considering both, fixed cameras [4] as well as on board cameras [6,25].

Commonly, as made in the above mentioned works, theoretical analysis about the stability of the servo visual control system is based on Lyapunov theory. An alternative choice is a passivity-based analysis, which has been applied to robotic manipulators control systems [8,16,22,27]. Recently, a useful dynamic model for unicycle-like mobile robots has been proposed in [21], proving also its passivity property. Additionally, a few recent works report control algorithms for mobile robots based on passivity theory, solving the path following problem [7], parking problem [18], and for coordinate muti-robots systems [1,13,14]. Also the locomotion problem of biped robots has been addressed using passivity theory [28]. On the topic of vision systems applied to mobile robots, [9,17] present a passivity based visual motion observer for mobile robots control purposes.

Regarding above mentioned works about passivity approaches, [8] is one of the most relevant papers in vision based controller design using passivity properties. However, authors use the passivity properties of the system in the context of a Lyapunov based

* Corresponding author at: Instituto de Automática (INAUT), Universidad Nacional de San Juan, Argentina.
E-mail addresses: bmorales@inaut.unsj.edu.ar (B. Morales), froberti@inaut.unsj.edu.ar (F. Roberti), mtoibero@inaut.unsj.edu.ar (J.M. Toibero), rcarelli@inaut.unsj.edu.ar (R. Carelli).

0957-4158/$ - see front matter © 2011 Elsevier Ltd. All rights reserved.
doi:10.1016/j.mechatronics.2011.09.007

stability proof, instead of an input–output analysis. On the topic of mobile robots, [7] presents a passivity based solution for the path following problem. Main disadvantage of this proposal is that it only applies for circular paths and only simulation results are presented. As mentioned in previous paragraph, [13] reports a passivity based approach for 3D attitude coordination of muti-robot systems. Authors propose an angular velocity control law that results in the convergence of the orientations among the robots in the 3D space, and show its performance through both simulations and experimental results. The proposal is interesting in spite of the initial assumption that rotation matrices of all robots are positive definite. Closer to our work, [17] has recently presented an important contribution in the field of mobile robots with visual sensing, taking advantage of passivity properties. Although the main contribution of this work is the visual motion observer, it also presents the design of a pose controller for a mobile robot carrying a catadioptric camera. The stability of the proposed system is concluded based on a Lyapunov analysis by assuming a static target and experimental results are shown only for the visual observer.

In this work, an image-based visual servoing system with *on-board* camera, based on the passivity theory is proposed. The designed controller allows the mobile robot to track a moving object in the workspace. By using the passivity properties of the robot and vision system, it is proved the convergence to zero of the control errors when assuming a perfect knowledge of the object's velocity. Next, a robustness analysis including the object velocity estimation errors is performed based on L_2-gain performance, thus concluding that control errors are ultimately bounded under this realistic assumption. It is important to remark that, different from previous related works [8,16,17,22], the convergence to zero of the control errors are proved in a passivity and input–output systems framework, instead of using the Lyapunov theory. Additionally, a real tracker controller is proposed instead of a robust pose controller [8,9,16,17,22,27], which means that it is not necessary to assume a static target in order to prove passivity properties and the convergence to zero of the control errors. As a final comment, this work considers the mobile robot dynamics in the control system design, which represents an important difference when comparing with previous passivity approaches for mobile robots.

The rest of the paper is organized as follows. Section 2 introduces the kinematic and the dynamic models of the mobile robot considered. In Section 3 the image features vector is defined and Jacobian matrices of the vision system model are obtained considering a pin-hole camera. Section 4 describes the proposed control system including stability proof and the robustness analysis. Section 5 shows the experimental results and, finally, Section 6 states the conclusions of the work.

2. Mobile robot model

This paper considers a unicycle type mobile robot, which has two independently driven wheels on the same axle and a castor wheel, as shown in Fig. 1. The usual set of kinematics equations which describe the vehicle's position and heading in the plane, when considering the robot as a punctual mass located in a point C at the middle of the wheels axle, are [34],

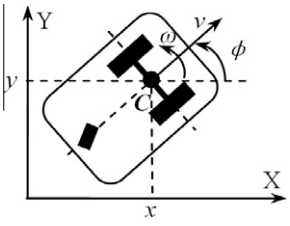

Fig. 1. Geometric description of the mobile robot.

$$\begin{aligned}\dot{x} &= v\cos\phi\\ \dot{y} &= v\sin\phi\\ \dot{\phi} &= \omega\end{aligned} \tag{1}$$

where (x,y) is the robot's position on a considered global framework, ϕ is the heading of the robot, v and ω are de linear and angular velocities, respectively.

The non-holonomic restriction of this kind of mobile robots is given by [34],

$$\dot{y}\cos\phi - \dot{x}\sin\phi = 0 \tag{2}$$

Intuitively, this constraint states that the robot cannot move laterally but it can only move in the direction normal to the axle of its driven wheels. The dynamic model will be described in Section 4.4, when presenting the dynamic compensation control.

3. Vision system model

A vision camera transforms a 3D space into a 2D projection on the image plane, where the vision sensor is located. Several projection models for the representation of the image formation process have been proposed [12]. The most used is the perspective projection model or pin-hole model. In this model, a coordinate system attached to the camera is defined in such a way that the X_{mc} and Y_{mc} axes define a base for the image plane and the Z_{mc} axis is parallel to the optic axis. The origin of the coordinate system is located at the focus of the camera lens. Then, a fixed point $\mathbf{P}$ in the 3D space with coordinates $\mathbf{P} = [x_{mc}\ y_{mc}\ z_{mc}]^T$ on the framework attached to the perspective camera will be projected on the image plane as a point with coordinates (x_m,y_m) given by [12]:

$$x_m = f\frac{x_{mc}}{z_{mc}};\quad y_m = f\frac{y_{mc}}{z_{mc}} \tag{3}$$

where f is the focal length of the camera, expressed in pixels.

3.1. Features selection

A feature parameter of the image is defined as any estimated real value that can be calculated from one or more structural components of the image. Some of the feature parameters more widely used are: the coordinates of a point on the image [10,24], the distance between two points on the image plane and the direction of the line connecting them, or the area of a projected surface as seen in [33].

Without loss of generality for the proposed control law, this work considers a cylindrical target, and the image features vector is defined as $\boldsymbol{\xi} = [\xi_1\ \xi_2]^T = [x_m\ d_m]^T$, being x_m the projection on the image plane of the x-coordinate of the cylinder middle point; and d_m is the projection on the image plane of the cylinder actual width D. This situation is represented in Fig. 2. The value of the image features is given by

$$x_m = f\frac{x_{Tmc}}{z_{Tmc}};\quad d_m = f\frac{D}{z_{Tmc}} \tag{4}$$

Note that expression for x_m is obtained directly from the first equation of (3) by replacing x and z coordinates of the generic point $\mathbf{P}$ by x_{Tmc} and z_{Tmc} (x and z coordinates of the target in the framework attached to the camera). On the other hand, d_m is obtained by writing $D = x_2 - x_1$, with x_1 and x_2 being the x-coordinates of two external points $\mathbf{P}_1$ and $\mathbf{P}_2$ of the target that define its diameter (as Fig. 2 shows). Then, the projections of x_1 and x_2 on the image plane are obtained through the first equation of (3). Finally, by subtracting these projections, second equation of (4) is obtained.

Now it is necessary to find the model of the vision system as a relation between the time variation of the image features vector $\dot{\xi}$

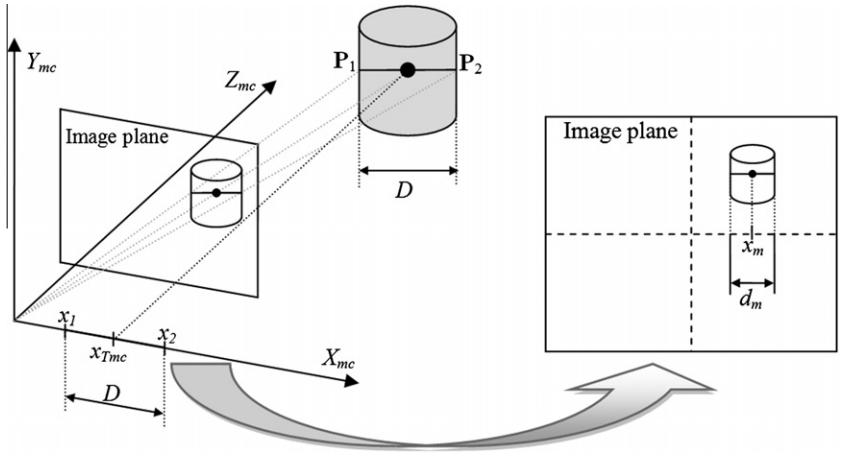

Fig. 2. Image features.

and the motion of both the mobile robot $[v\ \omega]^T$ and the target v_T. With this aim, let us consider the relative posture between the target and the vision system (on the plane $X_{mc} - Z_{mc}$ of the coordinate system attached to the camera) defined by the distance d and the angle φ, defined as shown in Fig. 3. Then, from this figure, the position of the target on the $X_{mc} - Z_{mc}$ plane is,

$$\begin{aligned} x_{Tmc} &= d\sin\varphi \\ z_{Tmc} &= d\cos\varphi \end{aligned} \tag{5}$$

Replacing (5) in (3), the image features vector is obtained as a function of the relative posture between the target and the camera (defined by distance d and angle φ)

$$\xi = \begin{bmatrix} f\tan\varphi & f\frac{D}{d\cos\varphi} \end{bmatrix}^T \tag{6}$$

and differentiating (6) with respect to time,

$$\dot{\xi} = \frac{\partial(\xi_1,\xi_2)}{\partial(\varphi,d)}\begin{bmatrix} \dot{\varphi} & \dot{d} \end{bmatrix}^T = \mathbf{J}_1\begin{bmatrix} \dot{\varphi} & \dot{d} \end{bmatrix}^T \tag{7}$$

$$\dot{\xi} = \begin{bmatrix} f\sec^2(\varphi) & 0 \\ \frac{fD}{d}\sec(\varphi)\tan(\varphi) & -\frac{fD}{d^2}\sec(\varphi) \end{bmatrix}\begin{bmatrix} \dot{\varphi} \\ \dot{d} \end{bmatrix} \tag{8}$$

$$\dot{\xi} = \mathbf{J}_1\begin{bmatrix} \dot{\varphi} & \dot{d} \end{bmatrix}^T$$

The change in relative position between the robot and the target is due to both, the robot motion and the target motion: $[\dot{\varphi}\ \dot{d}]^T = [\dot{\varphi}\ \dot{d}]_R^T + [\dot{\varphi}\ \dot{d}]_T^T$. Now, from the kinematics of the non holonomic mobile robot in polar coordinates (see Fig. 3) and first considering an static object, it is obtained the time variation of the relative posture between the target and the robot (time variation of d and φ) as a function of the linear and angular velocities of the robot as follows,

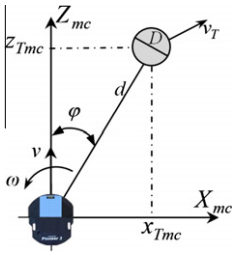

Fig. 3. Relative posture between the target and the robot.

$$\begin{bmatrix} \dot{\varphi} \\ \dot{d} \end{bmatrix}_R = \begin{bmatrix} \frac{\sin(\varphi)}{d} & 1 \\ -\cos(\varphi) & 0 \end{bmatrix}\begin{bmatrix} v \\ \omega \end{bmatrix} = \mathbf{J}_2\begin{bmatrix} v \\ \omega \end{bmatrix} \tag{9}$$

Considering now a fixed position for the mobile robot, i.e. constant values for x, y, ϕ; and differentiating (5) with respect to time, the target velocity $v_T = [\dot{x}_{Tmc}\ \dot{z}_{Tmc}]^T = \mathbf{A}[\dot{\varphi}\ \dot{d}]_T^T$ is obtained as,

$$v_T = \begin{bmatrix} d.\cos(\varphi) & \sin(\varphi) \\ -d.\sin(\varphi) & \cos(\varphi) \end{bmatrix}\begin{bmatrix} \dot{\varphi} \\ \dot{d} \end{bmatrix}_T \tag{10}$$

Then, since matrix **A** is invertible, it is possible to write

$$\begin{aligned} \begin{bmatrix} \dot{\varphi} \\ \dot{d} \end{bmatrix}_T &= \begin{bmatrix} \frac{1}{d}\cos(\varphi) & -\frac{1}{d}\sin(\varphi) \\ \sin(\varphi) & \cos(\varphi) \end{bmatrix} v_T \\ \begin{bmatrix} \dot{\varphi} & \dot{d} \end{bmatrix}_T^T &= \mathbf{J}_0 v_T \end{aligned} \tag{11}$$

Finally, by combining the movements of both the robot (9) and the target (11) into (8) the following expression for model of the vision system is obtained

$$\dot{\xi} = \mathbf{J}_1\left(\mathbf{J}_2[\,v\quad \omega\,]^T + \mathbf{J}_0[\,\dot{x}_{Tmc}\quad \dot{z}_{Tmc}\,]^T\right) \tag{12}$$

Defining

$$\begin{aligned} \mathbf{J} &= \mathbf{J}_1\mathbf{J}_2 \\ \mathbf{J}_T &= \mathbf{J}_1\mathbf{J}_0 \\ \boldsymbol{\mu} &= [\,v\quad \omega\,]^T \end{aligned} \tag{13}$$

a compact form for the vision system model is obtained,

$$\dot{\xi} = \mathbf{J}\boldsymbol{\mu} + \mathbf{J}_T v_T \tag{14}$$

where

$$\mathbf{J}_T = \begin{bmatrix} \frac{d_m}{D} & -\frac{d_m}{D}\frac{x_m}{f} \\ 0 & -\frac{d_m^2}{Df} \end{bmatrix} \tag{15}$$

$$\mathbf{J} = \begin{bmatrix} \frac{d_m x_m}{fD} & \frac{f^2+x_m^2}{f} \\ \frac{d_m^2}{Df} & \frac{d_m x_m}{f} \end{bmatrix} \tag{16}$$

4. Design of the passivity based visual controller

This section presents the design of an image-based visual controller to make a mobile robot with an on board camera capable to track a moving object on the workspace, making the image

features error $\tilde{\xi}(t)$ converge to zero. This way, the control objective is formally defined as follows,

$$\lim_{t\to\infty}\tilde{\xi}(t)=\mathbf{0}$$

First, a kinematics-based controller is designed and the convergence to zero of the image features error is proved when assuming perfect velocity tracking and perfect knowledge of the moving object velocity. Next, the perfect velocity tracking assumption is relaxed, and a dynamics-based controller is designed to verify the convergence to zero of the image features error under this realistic condition.

As mentioned in previous sections, full controller design is made in the context of the input–output systems theory, in particular by using the passivity properties of the system. This property has been widely used for the stability analysis of non linear systems [11], mainly for interconnected and cascade structured systems [2,23,32], as an alternative to Lyapunov theory. Formal definitions associated to passivity of operators relating functional spaces used in this work are given in Appendix.

4.1. Passivity property of the vision system

It has been proved in previous works that a perspective vision system located at the end effector of a robotic manipulator is passive when a punctual static object is considered [8]. This passivity property holds also when considering the vision system model (14), i.e. an on board camera in a mobile robot with a moving target.

Taking the positive function $V_\xi=\frac{1}{2}\xi^T\xi$, its time derivative is,

$$\dot{V}=\xi^T\dot{\xi}=\xi^T(\mathbf{J}\boldsymbol{\mu}+\mathbf{J}_T v_T) \tag{17}$$

Now, integrating (17) over [0,T],

$$\int_0^T\dot{V}dt=\int_0^T\xi^T(\mathbf{J}\boldsymbol{\mu}+\mathbf{J}_T v_T)dt-V(0)\leqslant V(T)-V(0)$$
$$=\int_0^T(\mathbf{J}^T\xi)^T(\boldsymbol{\mu}+\mathbf{J}^{-1}\mathbf{J}_T v_T)dt \tag{18}$$

defining $\upsilon_\xi=\mathbf{J}^T\xi$ and according with Definition A2, it can be concluded that mapping $(\boldsymbol{\mu}+\mathbf{J}^{-1}\mathbf{J}_T v_T)\to\upsilon_\xi$ is passive.

4.2. Design of the kinematic based controller

Considering now $\tilde{\xi}(t)=\xi(t)-\xi_{\mathbf{d}}$, instead of $\xi(t)$ in order to take into account the regulation problem on the image plane (being $\xi_{\mathbf{d}}$ the desired feature on the image plane), passivity property of the vision system holds. Let us take the following positive definite function

$$V=\int_0^{\tilde{\xi}^T}\boldsymbol{\eta}^T\mathbf{K}(\boldsymbol{\eta})\mathbf{d}\boldsymbol{\eta} \tag{19}$$

being $\mathbf{K}(\tilde{\xi})$ a positive definite gain matrix defined in order to avoid saturations as will be make clear later. Then, the time derivative of function V is $\dot{V}=\tilde{\xi}^T\mathbf{K}(\tilde{\xi})\dot{\tilde{\xi}}=\tilde{\xi}^T\mathbf{K}(\tilde{\xi})(\mathbf{J}\boldsymbol{\mu}+\mathbf{J}_T v_T)$. Integrating $\dot{V}$ over the interval [0,T],

$$\int_0^T\dot{V}dt=\int_0^T\tilde{\xi}^T\mathbf{K}(\tilde{\xi})(\mathbf{J}\boldsymbol{\mu}+\mathbf{J}_T v_T)dt \tag{20}$$

and defining

$$\upsilon_\xi=\mathbf{J}^T\mathbf{K}(\tilde{\xi})\tilde{\xi} \tag{21}$$

the following expression is obtained

$$\int_0^T\upsilon_\xi^T(\boldsymbol{\mu}+\mathbf{J}^{-1}\mathbf{J}_T v_T)dt\geqslant-V(0) \tag{22}$$

concluding that the mapping $(\boldsymbol{\mu}+\mathbf{J}^{-1}\mathbf{J}_T v_T)\to\upsilon_\xi$ is passive. At this point, it is important to express the conditions for matrix $\mathbf{K}(\tilde{\xi})$, which should be design such that $\upsilon_\xi\in L_\infty$ for any values of image features.

The following control law is proposed to track a moving target on the workspace, based on the error on the image plane.

$$\boldsymbol{\mu}_{\mathbf{ref}}^{\mathbf{c}}=-\mathbf{K}_{\mathbf{c}}\upsilon_\xi-\mathbf{J}^{-1}\mathbf{J}_T v_T=-\mathbf{K}_{\mathbf{c}}\mathbf{J}^T\mathbf{K}(\tilde{\xi})\tilde{\xi}-\mathbf{J}^{-1}\mathbf{J}_T v_T;\quad \mathbf{K}_{\mathbf{c}}>0 \tag{23}$$

Assuming for the moment perfect velocity tracking, i.e. $\boldsymbol{\mu}\equiv\boldsymbol{\mu}_{\mathbf{ref}}^{\mathbf{c}}$ (kinematics-based controller), and substituting (23) in (22),

$$\int_0^T\upsilon_\xi^T(\boldsymbol{\mu}+\mathbf{J}^{-1}\mathbf{J}_T v_T)dt=\int_0^T\upsilon_\xi^T(-\mathbf{K}_{\mathbf{c}}\upsilon_\xi-\mathbf{J}^{-1}\mathbf{J}_T v_T+\mathbf{J}^{-1}\mathbf{J}_T v_T)dt$$
$$=-\int_0^T\upsilon_\xi^T\mathbf{K}_{\mathbf{c}}\upsilon_\xi dt\leqslant-\lambda_{\min}(\mathbf{K}_{\mathbf{c}})\int_0^T\upsilon_\xi^T\upsilon_\xi dt \tag{24}$$

or

$$\int_0^T\upsilon_\xi^T(-\boldsymbol{\mu}-\mathbf{J}^{-1}\mathbf{J}_T v_T)dt\geqslant\lambda_{\min}(\mathbf{K}_{\mathbf{c}})\int_0^T\|\upsilon_\xi\|^2dt \tag{25}$$

Concluding that mapping $\upsilon_\xi\to-(\boldsymbol{\mu}+\mathbf{J}^{-1}\mathbf{J}_T v_T)$, i.e. the controller defined in (23), is strictly input passive (see Definition A3). This way, the proposed control system is made up by the interconnection of passive systems, as Fig. 4 shows.

4.3. Kinematic control system analysis

By adding (22) and (25)

$$0\geqslant-V(0)+\lambda_{\min}(\mathbf{K}_{\mathbf{c}})\int_0^T\|\upsilon_\xi\|^2dt$$
$$\int_0^T\|\upsilon_\xi\|^2dt\leqslant\frac{V(0)}{\lambda_{\min}(\mathbf{K}_{\mathbf{c}})} \tag{26}$$

which implies that $\upsilon_\xi\in L_{2e}$. Also, recalling that $\mathbf{K}(\tilde{\xi})$ is designed such that $\upsilon_\xi\in L_\infty$, and $\dot{\upsilon}_\xi\in L_\infty$ since robot velocities are also bounded (by controller definition (23)). Then, it can be concluded by Barbalat's Lemma [31] that

$$\upsilon_\xi\to\mathbf{0}\text{ with }t\to\infty \tag{27}$$

Now, assuming that the target is out of any singular position and recalling that, $\upsilon_\xi=\mathbf{J}^T\mathbf{K}(\tilde{\xi})\tilde{\xi}$, the condition (27) implies that,

$$\tilde{\xi}\to\mathbf{0}\text{ with }t\to\infty \tag{28}$$

thus achieving the control objective.

4.4. Design of the dynamic compensation

In this section the assumption of perfect velocity tracking is disregarded and a velocity controller considering the robot dynamics is designed and included in the proposed control system. This dynamic controller makes the robot to reach the reference velocity calculated by the kinematic controller with a good performance. This is particularly important under high velocity or heavy load conditions.

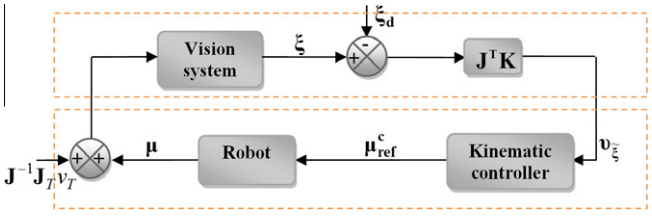

Fig. 4. Block diagram of the proposed kinematic visual control system.

This work considers the dynamic model proposed in [21],

$$\mathbf{H}\dot{\boldsymbol{\mu}} + \mathbf{C}(\boldsymbol{\mu})\boldsymbol{\mu} + \mathbf{F}(\boldsymbol{\mu})\boldsymbol{\mu} = \boldsymbol{\mu}_\mathbf{r} \tag{29}$$

where $\boldsymbol{\mu} = [v\ \omega]^T$ and $\boldsymbol{\mu}_\mathbf{r} = [v_r\ \omega_r]^T$ represent the vector of linear and angular input velocities. Matrix $\mathbf{H}$ is constant, diagonal and positive definite; matrix $\mathbf{C}(\boldsymbol{\mu})$ is skew symmetric; and matrix $\mathbf{F}(\boldsymbol{\mu})$ is (for reasonable assumptions) symmetric, positive definite and lower bounded. Furthermore, mapping $\boldsymbol{\mu}_\mathbf{r} \to \boldsymbol{\mu}$ is strictly output passive. For more details about dynamic model (29), refer to [21].

The following control law is proposed,

$$\boldsymbol{\mu}_\mathbf{r} = \mathbf{H}\dot{\boldsymbol{\mu}}^\mathbf{c}_\mathbf{ref} + \mathbf{C}(\boldsymbol{\mu})\boldsymbol{\mu}^\mathbf{c}_\mathbf{ref} + \mathbf{F}(\boldsymbol{\mu})\boldsymbol{\mu}^\mathbf{c}_\mathbf{ref} - \mathbf{T}(\tilde{\boldsymbol{\mu}}) \tag{30}$$

$$\tilde{\boldsymbol{\mu}} = \boldsymbol{\mu} - \boldsymbol{\mu}^\mathbf{c}_\mathbf{ref} = [\,\tilde{v}\quad \tilde{\omega}\,]^T \tag{31}$$

$$\mathbf{T}(\tilde{\boldsymbol{\mu}}) = \begin{bmatrix} l_v & 0 \\ 0 & l_\omega \end{bmatrix} \left[\, tgh\left(\tfrac{k_v}{l_v}\tilde{v}\right) \quad tgh\left(\tfrac{k_\omega}{l_\omega}\tilde{\omega}\right) \right]^T \tag{32}$$

where hyperbolic tangent function prevents the saturation of the control commands due to large velocity errors; $k_v,\ k_\omega > 0;\ l_v,\ l_\omega \in \Re$. The new block diagram of the proposed control system is depicted in Fig. 5.

4.5. Stability proof of the complete proposed control system

Replacing (30) into (29), the following close loop equation is obtained,

$$\mathbf{H}\dot{\tilde{\boldsymbol{\mu}}} + \mathbf{C}(\boldsymbol{\mu})\tilde{\boldsymbol{\mu}} + \mathbf{F}(\boldsymbol{\mu})\tilde{\boldsymbol{\mu}} = -\mathbf{T}(\tilde{\boldsymbol{\mu}}) \tag{33}$$

For stability analysis purposes, let us consider the following positive definite function,

$$V = \frac{1}{2}\tilde{\boldsymbol{\mu}}^T\mathbf{H}\tilde{\boldsymbol{\mu}} \tag{34}$$

and its time derivative on the system trajectories,

$$\dot{V} = -\tilde{\boldsymbol{\mu}}^T\mathbf{C}(\boldsymbol{\mu})\tilde{\boldsymbol{\mu}} - \tilde{\boldsymbol{\mu}}^T\mathbf{F}(\boldsymbol{\mu})\tilde{\boldsymbol{\mu}} - \tilde{\boldsymbol{\mu}}^T\mathbf{T}(\tilde{\boldsymbol{\mu}}) \tag{35}$$

The first term is zero since $\mathbf{C}(\boldsymbol{\mu})$ is skew symmetric, the second one is negative definite since $\mathbf{F}(\boldsymbol{\mu})$ is symmetric and third term is negative definite (see definition of $\mathbf{T}(\tilde{\boldsymbol{\mu}})$ in (32)), therefore $\dot{V} < 0$. Then, it can be concluded that,

$$\tilde{\boldsymbol{\mu}} \in L_\infty \tag{36}$$

Integrating $\dot{V}$ over the interval $[0,T]$,

$$\int_0^T \dot{V}dt = -\int_0^T \tilde{\boldsymbol{\mu}}^T\mathbf{F}(\boldsymbol{\mu})\tilde{\boldsymbol{\mu}}dt - \int_0^T \tilde{\boldsymbol{\mu}}^T\mathbf{T}(\tilde{\boldsymbol{\mu}})dt \tag{37}$$

or $-V(0) \leqslant -\int_0^T \tilde{\boldsymbol{\mu}}^T\mathbf{T}(\tilde{\boldsymbol{\mu}})dt - \int_0^T \tilde{\boldsymbol{\mu}}^T\mathbf{F}\tilde{\boldsymbol{\mu}}dt$, by recalling that $V(T) > 0$. Rewriting previous expression as,

$$-\int_0^T \tilde{\boldsymbol{\mu}}^T\mathbf{T}(\tilde{\boldsymbol{\mu}})dt \geqslant -V(0) + \lambda_{\min}(\mathbf{F})\|\tilde{\boldsymbol{\mu}}\|^2 \tag{38}$$

it can be concluded that the mapping $-\mathbf{T}(\tilde{\boldsymbol{\mu}}) \to \tilde{\boldsymbol{\mu}}$ is strictly output passive.

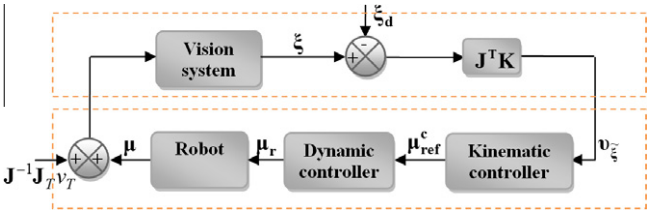

Fig. 5. Block diagram of the proposed control system with dynamic compensation.

Now, by recalling (36), there exists a constant matrix $\mathbf{K_T}$ such that $\tilde{\boldsymbol{\mu}}^T\mathbf{T}(\tilde{\boldsymbol{\mu}}) \geqslant \lambda_{min}(\mathbf{K_T})\tilde{\boldsymbol{\mu}}^T\tilde{\boldsymbol{\mu}}$ in domain of $\tilde{\boldsymbol{\mu}}$ so, from (37) the following expression is obtained,

$$-V(0) \leqslant -\lambda_{\min}(\mathbf{K_T})\int_0^T \tilde{\boldsymbol{\mu}}^T\tilde{\boldsymbol{\mu}}dt - \int_0^T \tilde{\boldsymbol{\mu}}^T\mathbf{F}\tilde{\boldsymbol{\mu}}dt \tag{39}$$

It can also be written,

$$\begin{aligned} &V(0) \geqslant (\lambda_{\min}(\mathbf{K_T}) + \lambda_{\min}(\mathbf{F}))\int_0^T \tilde{\boldsymbol{\mu}}^T\tilde{\boldsymbol{\mu}}dt \\ &\int_0^T \tilde{\boldsymbol{\mu}}^T\tilde{\boldsymbol{\mu}}dt \leqslant \frac{V(0)}{(\lambda_{\min}(\mathbf{K_T}) + \lambda_{\min}(\mathbf{F}))}\forall T \in [0,\infty) \Rightarrow \tilde{\boldsymbol{\mu}} \in L_2 \end{aligned} \tag{40}$$

Now, after proving that $\tilde{\boldsymbol{\mu}} \in [L_2 \cap L_\infty]$, the control error $\tilde{\boldsymbol{\xi}}$ has to be analyzed. With this aim, the assumption of perfect velocity tracking is disregarded, thus considering a nonzero velocity error $\tilde{\boldsymbol{\mu}} = \boldsymbol{\mu} - \boldsymbol{\mu}^\mathbf{c}_\mathbf{ref}$. This velocity error and the kinematic controller are introduced into (24), obtaining

$$-\int_0^T \boldsymbol{\upsilon}^T_{\tilde{\boldsymbol{\xi}}}(\boldsymbol{\mu} + \mathbf{J}^{-1}\mathbf{J}_T v_T)dt = \int_0^T \boldsymbol{\upsilon}^T_{\tilde{\boldsymbol{\xi}}}\mathbf{K_c}\boldsymbol{\upsilon}_{\tilde{\boldsymbol{\xi}}}dt - \int_0^T \boldsymbol{\upsilon}^T_{\tilde{\boldsymbol{\xi}}}\tilde{\boldsymbol{\mu}}dt \tag{41}$$

Then, by adding (41) with the expression that states the passivity property of the vision system (22) and after some manipulations, the following expression is obtained,

$$\lambda_{\min}(\mathbf{K_c})\int_0^T \boldsymbol{\upsilon}^T_{\tilde{\boldsymbol{\xi}}}\boldsymbol{\upsilon}_{\tilde{\boldsymbol{\xi}}}dt \leqslant V(0) + \int_0^T \boldsymbol{\upsilon}^T_{\tilde{\boldsymbol{\xi}}}\tilde{\boldsymbol{\mu}}dt \tag{42}$$

$$\lambda_{\min}(\mathbf{K_c})\|\boldsymbol{\upsilon}_{\tilde{\boldsymbol{\xi}}}\|^2_{2T} \leqslant V(0) + \|\boldsymbol{\upsilon}_{\tilde{\boldsymbol{\xi}}}\|_{2T}\|\tilde{\boldsymbol{\mu}}\|_{2T} \qquad \forall T \in [0,\infty) \tag{43}$$

By recalling that $\tilde{\boldsymbol{\mu}} \in L_2$(40), inequality (43) only holds for $\|\boldsymbol{\upsilon}_{\tilde{\boldsymbol{\xi}}}\|_{2T} < \infty$, which implies that $\boldsymbol{\upsilon}_{\tilde{\boldsymbol{\xi}}} \in L_2$. This conclusion shows that the property $\boldsymbol{\upsilon}_{\tilde{\boldsymbol{\xi}}} \in L_2$ remains valid after including the dynamical velocity controller when disregarding the assumption of perfect velocity tracking. Remembering that $\boldsymbol{\upsilon}_{\tilde{\boldsymbol{\xi}}} \in L_\infty$ and $\dot{\boldsymbol{\upsilon}}_{\tilde{\boldsymbol{\xi}}} \in L_\infty$, then the control objective is achieved, i.e.

$$\tilde{\boldsymbol{\xi}}(t) \to \mathbf{0} \text{ with } t \to \infty \tag{44}$$

4.6. Robustness analysis

Control action defined by (23) assumes the perfect knowledge of the moving object velocity v_T, but in practice this velocity will be estimated by using the visual position sensing of the object though, for instance, an $\alpha - \beta$ filter [15]. The estimation of the object velocity immediately raises the problem of analyzing the effect of the estimation error on the control errors.

In this analysis, the L_2-gain performance criterion will be used. With this aim, estimation error of the target velocity $\tilde{v}_T$ and velocity error $\tilde{\boldsymbol{\mu}}$ will be considered as parts of an external disturbance $\mathbf{w}$ and it will be proved that the mapping from $\mathbf{w}$ to $\tilde{\boldsymbol{\xi}}$ has finite L_2-gain, i.e. [30],

$$\int_0^T \|\tilde{\boldsymbol{\xi}}\|^2dt < \gamma^2\int_0^T \|\mathbf{w}\|^2dt \quad \forall T > 0 \tag{45}$$

Let us define the external disturbance as $\mathbf{w} = \tilde{\boldsymbol{\mu}} + \mathbf{J}^{-1}\mathbf{J_T}\tilde{v}_T$, being $\tilde{v}_T = v_T - \hat{v}_T$, and assume that $\mathbf{w}$ is bounded. Considering now that the velocity of the target is not perfectly known in the expression of the controller (23) and (24) is modified as follows,

$$\begin{aligned} \int_0^T \boldsymbol{\upsilon}^T_{\tilde{\boldsymbol{\xi}}}(\boldsymbol{\mu} + \mathbf{J}^{-1}\mathbf{J}_T v_T)dt &= \int_0^T \boldsymbol{\upsilon}^T_{\tilde{\boldsymbol{\xi}}}(\tilde{\boldsymbol{\mu}} + \boldsymbol{\mu}^\mathbf{c}_\mathbf{ref} + \mathbf{J}^{-1}\mathbf{J}_T v_T)dt \\ &= \int_0^T \boldsymbol{\upsilon}^T_{\tilde{\boldsymbol{\xi}}}\tilde{\boldsymbol{\mu}}dt - \int_0^T \boldsymbol{\upsilon}^T_{\tilde{\boldsymbol{\xi}}}\mathbf{K_c}\boldsymbol{\upsilon}_{\tilde{\boldsymbol{\xi}}}dt \\ &\quad + \int_0^T \boldsymbol{\upsilon}^T_{\tilde{\boldsymbol{\xi}}}(-\mathbf{J}^{-1}\mathbf{J}_T\hat{v}_T + \mathbf{J}^{-1}\mathbf{J}_T v_T)dt \end{aligned} \tag{46}$$

$$\int_0^T \boldsymbol{\upsilon}_{\tilde{\xi}}^T(\boldsymbol{\mu}+\mathbf{J}^{-1}\mathbf{J}_T\upsilon_T)dt = -\int_0^T \boldsymbol{\upsilon}_{\tilde{\xi}}^T\mathbf{K_c}\boldsymbol{\upsilon}_{\tilde{\xi}}dt + \int_0^T \boldsymbol{\upsilon}_{\tilde{\xi}}^T\tilde{\boldsymbol{\mu}}dt + \int_0^T \boldsymbol{\upsilon}_{\tilde{\xi}}^T\mathbf{J}^{-1}\mathbf{J}_T\tilde{\upsilon}_T dt \quad (47)$$

$$\int_0^T \boldsymbol{\upsilon}_{\tilde{\xi}}^T(\boldsymbol{\mu}+\mathbf{J}^{-1}\mathbf{J}_T\upsilon_T)dt = -\int_0^T \boldsymbol{\upsilon}_{\tilde{\xi}}^T\mathbf{K_c}\boldsymbol{\upsilon}_{\tilde{\xi}}dt + \int_0^T \boldsymbol{\upsilon}_{\tilde{\xi}}^T\mathbf{w}dt \quad (48)$$

By subtracting (48) from (21), the following expression is obtained,

$$0 \geqslant -V(0) + \int_0^T \boldsymbol{\upsilon}_{\tilde{\xi}}^T\mathbf{K_c}\boldsymbol{\upsilon}_{\tilde{\xi}}dt - \int_0^T \boldsymbol{\upsilon}_{\tilde{\xi}}^T\mathbf{w}dt \quad (49)$$

Then,

$$\lambda_{\min}(\mathbf{K_c})\int_0^T \boldsymbol{\upsilon}_{\tilde{\xi}}^T\boldsymbol{\upsilon}_{\tilde{\xi}}dt \leqslant V(0) + \int_0^T \boldsymbol{\upsilon}_{\tilde{\xi}}^T\mathbf{w}dt \quad (50)$$

or, by defining $\varepsilon = \lambda_{\min}(\mathbf{K_c})$ and recalling the definition of the inner product in the space L_{2e} (see Definition A1),

$$\varepsilon\|\boldsymbol{\upsilon}_{\tilde{\xi}}\|_{2T}^2 \leqslant \langle \boldsymbol{\upsilon}_{\tilde{\xi}}^T, \mathbf{w}\rangle_T + V(0) \quad (51)$$

Now, by adding to the second member of (51) the positive term $\frac{1}{2}\left\langle \frac{1}{\sqrt{\varepsilon}}\mathbf{w} - \sqrt{\varepsilon}\boldsymbol{\upsilon}_{\tilde{\xi}}^T, \frac{1}{\sqrt{\varepsilon}}\mathbf{w} - \sqrt{\varepsilon}\boldsymbol{\upsilon}_{\tilde{\xi}}^T\right\rangle_T$, the inequality holds. After some mathematical manipulations, the following expression is obtained,

$$\varepsilon\|\boldsymbol{\upsilon}_{\tilde{\xi}}\|_{2T}^2 \leqslant \left\langle \boldsymbol{\upsilon}_{\tilde{\xi}}^T, \mathbf{w}\right\rangle_T + \frac{1}{2}\frac{1}{\varepsilon}\langle \mathbf{w}, \mathbf{w}\rangle_T + \frac{\varepsilon}{2}\left\langle \boldsymbol{\upsilon}_{\tilde{\xi}}^T, \boldsymbol{\upsilon}_{\tilde{\xi}}^T\right\rangle_T - \left\langle \boldsymbol{\upsilon}_{\tilde{\xi}}^T, \mathbf{w}\right\rangle_T + V(0) \quad (52)$$

$$\|\boldsymbol{\upsilon}_{\tilde{\xi}}\|_{2T}^2 \leqslant \frac{1}{\varepsilon^2}\|\mathbf{w}\|_{2T}^2 + V(0) \quad (53)$$

Now, for $\|\mathbf{w}\|_2^2$ such that $\|\boldsymbol{\upsilon}_{\tilde{\xi}}\|_2^2$ be bounded away from its saturation value, and after replacing (21) into (53) it can be concluded that,

$$\|\tilde{\boldsymbol{\xi}}^T\|_{2T}^2 \leqslant \frac{1}{\lambda_{\min}(\mathbf{M})\varepsilon^2}\|\mathbf{w}\|_{2T}^2 + V(0) \quad (54)$$

where $\mathbf{M} = \mathbf{K}^T(\tilde{\boldsymbol{\xi}})\mathbf{J}\mathbf{J}^T\mathbf{K}(\tilde{\boldsymbol{\xi}})$.

Clearly, after integrating (54) over the interval $[0,T]$, it can be concluded that the mapping from $\mathbf{w}$ to $\tilde{\boldsymbol{\xi}}$ has finite L_2-gain $\leqslant\gamma$, with $\gamma = \frac{1}{\varepsilon\sqrt{\lambda_{min}(\mathbf{M})}}$. In other words, the proposed control system is robust to $\mathbf{w}$ according to L_2-performance criterion (disturbance attenuation in L_2-gain norm or energy attenuation). In this context, the parameter γ can be considered as an indicator of the control system performance in presence of estimation errors.

5. Experimental results

The proposed visual controller has been evaluated through real experiments using a Pioneer 3DX manufactured by MobileRobots Inc., with on-board computer and color CCD camera (with focal distance $f = 850$ pixels). For the cases of moving target experiments, the cylindrical target has been placed on another mobile platform Pioneer 3AT. Experimental setup is shown in Fig. 6.

Three different indoor experiments are shown, the first one with a static target and the other two considering a moving target. It is important to test these two conditions since the controller should present a good performance in spite of different target velocities. Two velocity conditions are used in the second and third experiments. For all experiments, the target velocity is considered as unknown and it is estimated by using an $\alpha-\beta$ filter [15]. Nevertheless, any other adequate velocity estimation algorithm could be implemented.

Matrix $\mathbf{K}(\tilde{\xi})$ was defined as,

Fig. 6. Experimental setup.

$$\mathbf{K}(\tilde{\boldsymbol{\xi}}) = diag\left(\frac{k_1}{(a_1+|\tilde{\xi}_1|)(b_1+d_m)(c_1+|x_m|^2)}, \frac{k_2}{(a_2+|\tilde{\xi}_2|)\left(b_2+d_m^2\right)(c_2+|x_m|)}\right)$$
$$k_i, a_i, b_i, c_i > 0$$

This matrix has been designed such that $\boldsymbol{\upsilon}_{\tilde{\xi}} \in L_\infty$ as expressed in Section 4.2. Note that it depends on the Jacobian matrix associated to the defined image features. With this matrix $\mathbf{K}(\tilde{\xi})$, the following expression for $\boldsymbol{\upsilon}_{\tilde{\xi}}$ is obtained,

$$\boldsymbol{\upsilon}_{\tilde{\xi}} = \begin{bmatrix} \frac{k_1 d_m x_m \tilde{\xi}_1}{fD(a_1+|\tilde{\xi}_1|)(b_1+d_m)(c_1+|x_m|^2)} + \frac{k_2 d_m^2 \tilde{\xi}_2}{fD(a_2+|\tilde{\xi}_2|)\left(b_2+d_m^2\right)(c_2+|x_m|)} \\ \frac{k_1\left(f^2+x_m^2\right)\tilde{\xi}_1}{D(a_1+|\tilde{\xi}_1|)(b_1+d_m)(c_1+|x_m|^2)} + \frac{k_2 d_m x_m \tilde{\xi}_2}{f(a_2+|\tilde{\xi}_2|)\left(b_2+d_m^2\right)(c_2+|x_m|)} \end{bmatrix} \in L_\infty$$

The design constants of the proposed controllers are set to: $k_1 = 0.25$, $k_2 = 15$, $a_1 = 70$, $a_2 = 100$, $b_1 = 20$, $c_1 = 30$, $b_2 = 30$, $c_2 = 20$, $\mathbf{K_c} = diag(70,4)$, $l_v = 0.01$, $k_v = 0.05$, $l_\omega = 0.03$, $k_\omega = 0.12$; and the desired features vector is selected as $\boldsymbol{\xi_d} = [0\ 270]^T$ for the first experiment and $\boldsymbol{\xi_d} = [0\ 170]^T$ for the second and third experiment. Note that transforming these desired image features into relative posture between the robot and the target, $d = 0.63$ m and $\varphi = 0°$ can be obtained for the first experiment; and $d = 1$ m and $\varphi = 0°$ for the second and third ones. In spite of these values of relative posture are not used for control purposes; they can be useful for the results interpretation.

In the first experiment, a static target is considered. Therefore, the robot has to achieve a final position relative to the target, according to the desired visual features vector. Figs. 7–10 show the obtained results. Fig. 7 represents the time evolution of the visual features errors, Fig. 8 shows the time evolution of control actions, Fig. 9 depicts the trajectory described by the robot in the workspace, and Fig. 10 illustrates the evolution of the relative position between the robot and the target.

In the second experiment, the target moves in the workspace with constant velocity describing a straight line path. Therefore, the robot has to track the target while keeping a constant relative posture to the target. Similar to previous experiment, Figs. 11–14 show the obtained results. Fig. 11 represents the time evolution of the visual features errors, Fig. 12 shows the time evolution of control actions, Fig. 13 depicts the trajectories described by both the moving target and the robot in the workspace, and Fig. 14 illustrates the evolution of the relative position between the robot and the target.

In the last experiment presented in this Section, the target also moves in the workspace but with non-constant velocity. Fig. 15

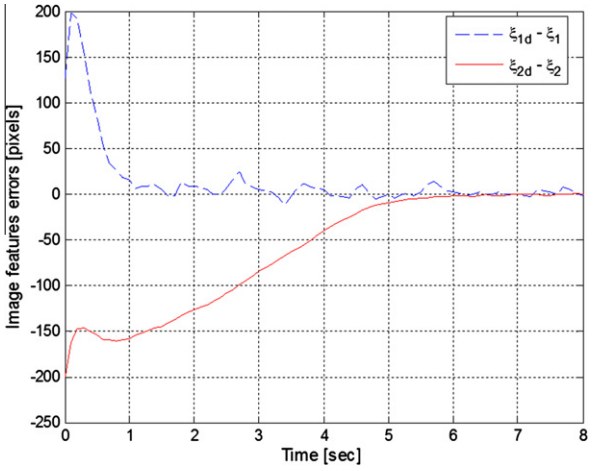

Fig. 7. Time evolution of the image features error (first experiment).

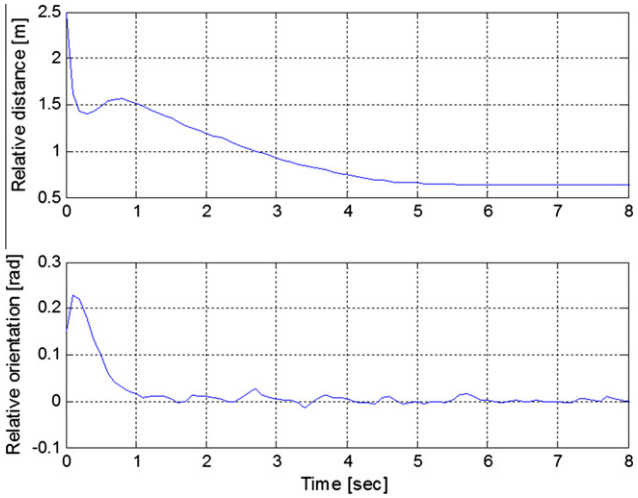

Fig. 10. Relative posture between the robot and the target (first experiment).

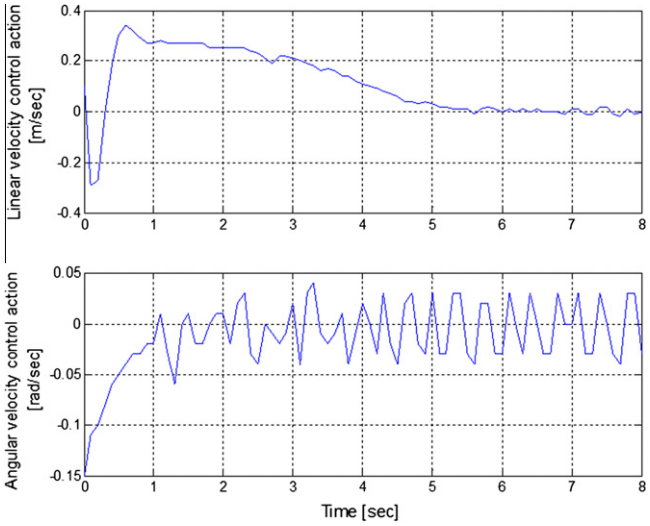

Fig. 8. Time evolution of the control commands (first experiment).

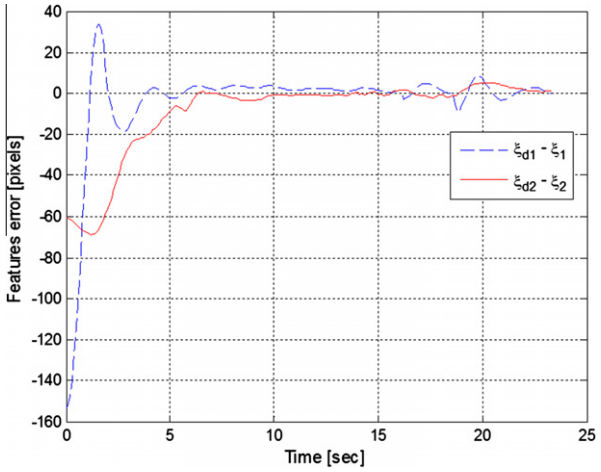

Fig. 11. Time evolution of the image features error (second experiment).

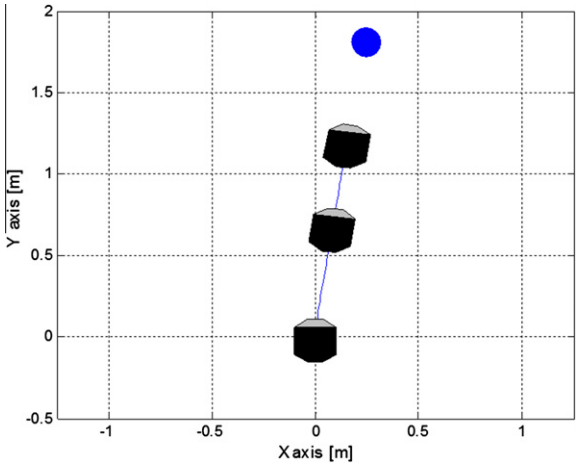

Fig. 9. Trajectory described by the robot in the workspace (first experiment).

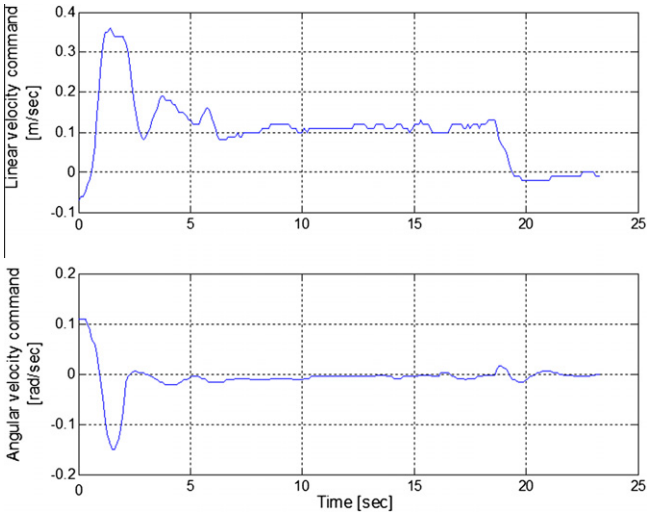

Fig. 12. Time evolution of the control commands (second experiment).

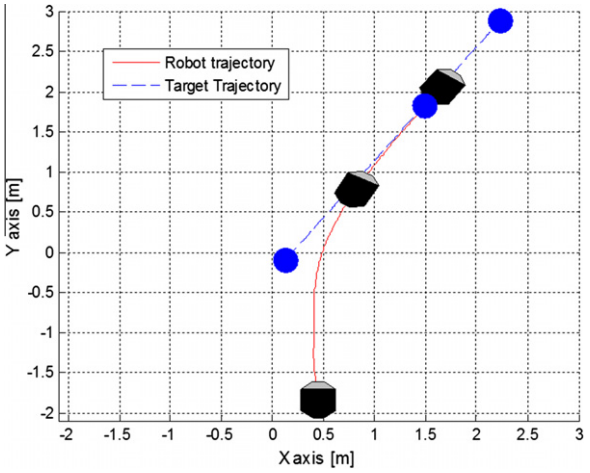

Fig. 13. Trajectories described by the robot and the target in the workspace (second experiment).

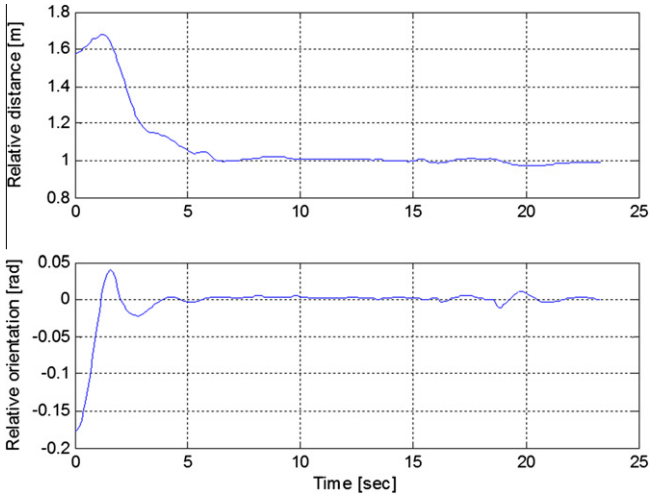

Fig. 14. Relative posture between the robot and the target (second experiment).

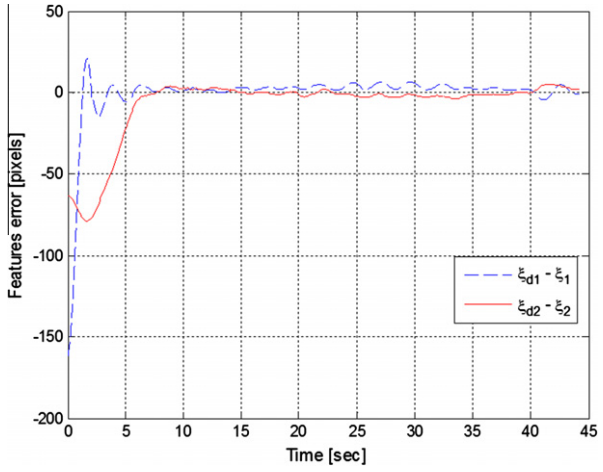

Fig. 15. Time evolution of the image features error (third experiment).

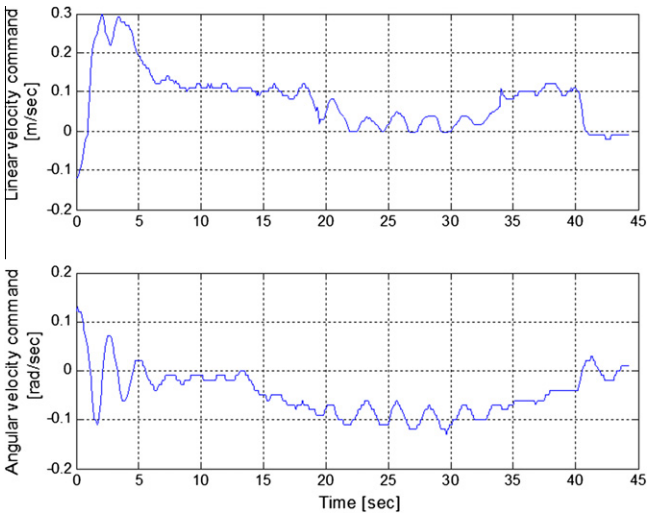

Fig. 16. Time evolution of the control commands (third experiment).

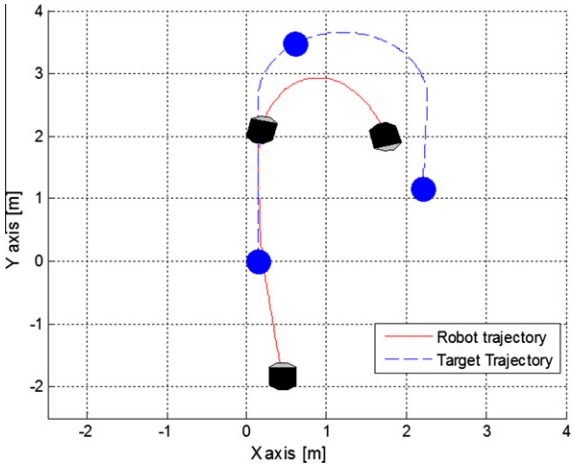

Fig. 17. Trajectories described by the robot and the target in the workspace (third experiment).

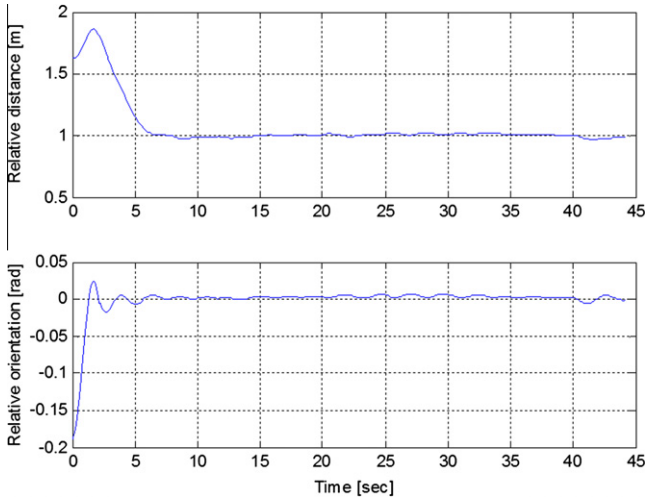

Fig. 18. Relative posture between the robot and the target (third experiment).

shows the time evolution of the visual features errors, Fig. 16 represents the time evolution of control actions, Fig. 17 depicts the trajectories described both by the mobile target and the robot in the workspace, and Fig. 18 illustrates the evolution of the relative position between the robot and the target.

All the experiments have shown the feasibility of the implementation and the good performance of the proposed controller. It can be seen how the proposed controller makes the robot able to get a desired posture relative to the static target (experiment 1), as well as to follow a moving target (experiments 2 and 3), achieving similar performances. Even with non-constant target's velocity the performance is not affected, as experiment 3 shows.

It is important to highlight that, in spite of the unknown target's velocity; the proposed controller reduces the control errors down to values close to zero. This behavior confirms the theoretical results regarding not only the asymptotic stability property but also the robustness of the proposed controller against the errors in the estimation of the target's velocity. Remember that this velocity has been estimated through the visual sensing by using a standard estimation algorithm.

6. Conclusions

In this paper, an image-based visual controller for object tracking with on board camera has been presented. First, a kinematics-based controller was proposed and the asymptotically convergence to zero of the control errors has been proved assuming perfect velocity tracking. Then, a more realistic situation by considering the velocity error motivates the design of a dynamics-based velocity controller, and the convergence to zero of the image features error is proved again for the control system. The dynamics-based controller receives the velocity references values from the kinematics-based one. The design of the proposed control system is based on its passivity properties and the input–output systems theory. Finally, estimation errors on the target velocity have been considered, and a robustness analysis allows to conclude that the control system is robust to these errors according the L_2-gain performance criterion. Experimental results were also presented in order to validate the proposed controller.

Appendix A

Formal definitions associated to passivity of operators relating functional spaces and used in this work follow [30].

Definition A1. Given g, $h \in L_{2e}$, the inner product and the norm $\|\bullet\|_{2e}$ in the set L_{2e} are defined as,

$$\langle g, h\rangle_T = \int_0^T g(t)h(t)dt \quad \forall T \in [0,\infty)$$
$$\|g\|_{2,T} = \langle g, g\rangle_T^{1/2} = \left(\int_0^T g(t)g(t)dt\right)^{1/2}$$

Definition A2. Let $\mathbf{G}$:$L_{2e} \to L_{2e}$ be an input–output mapping. Then, $\mathbf{G}$ is *passive* if there exists some constant β such that,

$$\langle \mathbf{Gx}, \mathbf{x}\rangle_T \geqslant \beta \ \forall \mathbf{x} \in L_{2e} \quad \forall T \in [0,\infty)$$

Definition A3. Let $\mathbf{G}$:$L_{2e} \to L_{2e}$ be an input–output mapping. Then, $\mathbf{G}$ is *strictly input passive* if there exists some constants $\beta \in \Re$ and $\delta > 0$ such that,

$$\langle \mathbf{Gx}, \mathbf{x}\rangle_T \geqslant \beta + \delta\|\mathbf{x}\|_{2,T}^2 \quad \forall \mathbf{x} \in L_{2e}$$

Definition A4. Let $\mathbf{G}$:$L_{2e} \to L_{2e}$ be an input–output mapping. Then, $\mathbf{G}$ is *strictly output passive* if there exists some constants $\beta \in \Re$ and $\delta > 0$ such that,

$$\langle \mathbf{Gx}, \mathbf{x}\rangle_T \geqslant \beta + \delta\|\mathbf{Gx}\|_{2,T}^2 \quad \forall \mathbf{x} \in L_{2e}$$

References

[1] Arcak M. Passivity as a design tool for group coordination. IEEE Trans Auto Control 2007;52(8):1380–90.
[2] Bynes CI, Isidori A, Willems JC. Passivity, feedback equivalence, and the global stabilization of minimum phase nonlinear systems. IEEE Trans Auto Control 1991;36(11):1228–40.
[3] Carelli R, Kelly R, Nasisi OH, Soria C, Mut V. Control based on perspective lines of a nonholonomic mobile robot with camera-on-board. Int J Control 2006;79:362–71.
[4] Carelli R, De la Cruz C, Roberti F. Centralized formation control of non-holonomic mobile robots. Latin Am Appl Res 2006;36(2):63–9.
[5] Carelli R, Santos-Victor J, Roberti F, Tosetti S. Direct visual tracking control of remote cellular robots. Robot Autonom Syst 2006;54(10):805–14.
[6] Das AK, Fierro R, Kumar V, Ostrowski JP, Spletzer J, Taylor CJ. A vision-based formation control framework. IEEE Trans Robot Autom 2002;18(5):813–25.
[7] El-Hawwary MI, Maggiore, M. Global path following for the unicycle and other results. In: American control conference; 11–13 June 2008. p. 3500–5.
[8] Fujita M, Kawai H, Spong MW. Passivity-based dynamic visual feedback control for three dimensional target tracking: stability and L2-gain performance analysis. IEEE Trans Control Syst Technol 2007;15(1):40–52.
[9] Fujita M, Hatanaka T, Kobayashi N, Ibuki T, Spong M. Visual motion observer-based pose synchronization: a passivity approach. In: Proceedings of the IEEE international conference on decision and control. Shanghai, China; 2009. p. 2402–7.
[10] Hashimoto K. Visual servoing real time control of robot manipulators based on visual sensory feedback. World Scient Series Robot Autom Syst 1993;7:139–64.
[11] Hill D, Moylan P. Stability results for nonlinear feedback systems. Automática 1976;13:373–82.
[12] Hutchinson S, Hager G, Corke P. A tutorial on visual servo control. IEEE Trans Robot Autom 1996;12(5):651–70.
[13] Igarashi Y, Hatanaka T, Fujita M, Spong MW. Passivity-based 3D attitude coordination: convergence and connectivity. In: IEEE conference on decision and control; 2007. p. 2558–65.
[14] Ihle I, Arcak M, Fossen T. Passivity-based designs for synchronized path-following. Automatica 2007;43(9):1508–18.
[15] Kalata P. The tracking index: a generalized parameter for $\alpha-\beta$ and $\alpha-\beta-\gamma$ target trackers. IEEE Trans Aerosp Electr Syst 1994;20(2):174–82.
[16] Kawai H, Toshiyuki M, Fujita M. Image-based dynamic visual feedback control via passivity approach. In: Proceedings of the IEEE international conference on control applications. Munich, Germany; 2006. p. 740–5.
[17] Kawai H, Murao T, Fujita M. Passivity-based visual motion observer with panoramic camera for pose control. J Intell Robot Syst, in press. Doi: doi:10.1007/s10846-011-9557-5.
[18] Lee D. Passivity-based switching control for stabilization of wheeled mobile robots. Proc Robot Sci Syst 2007.
[19] López-Nicolás G, Guerrero JJ, Sagüés C. Visual control of vehicles using two-view geometry. Mechatronics 2010;20(2):315–25.
[20] López-Nicolás G, Guerrero JJ, Sagüés C. Visual control through the trifocal tensor for nonholonomic robots. Robot Autonom Syst 2010;58(2):216–26.
[21] Martins F, Sarcinelli M, Freire Bastos T, Carelli R. Dynamic modeling and trajectory tracking control for unicycle-like mobile robots. In: 3rd International symposium on multibody systems and mechatronics. San Juan, Argentina; 2008.
[22] Murao T, Kawai H, Fujita M. Passivity-based dynamic visual feedback control with a movable camera. In: 44th IEEE international conference on decision and control. Spain; 2005. p. 5360–5.
[23] Ortega R, Loria A, Nelly R, Praly L. On passivity based output feedback global stabilization of Euler–Lagrange systems. Int J Robust Nonlin Control 1995;5:313–24.
[24] Papanikolopoulos NP, Khosla PK, Kanade T. Visual tracking of a moving target by a camera mounted on a robot: a combination of control and vision. IEEE Trans Robot Automa 1993;9(1):14–35.
[25] Roberti F, Toibero JM, Soria C, Vassallo R, Carelli R. Hybrid collaborative stereo vision system for mobile robots formation. Int J Adv Robot Syst 2009;6(4):257–66.
[26] Santos-Victor J. Vision based remote control of cellular robots. Robot Autonom Syst 1998;23(4):221–34.
[27] Soria C, Roberti F, Carelli R, Sebastián JM. Control servo-visual de un robot manipulador planar basado en pasividad. Revista Iberoamericana de Automática e Informática Industrial 2008;5(4):54–61.
[28] Spong MW, Holm JK, Lee DJ. Passivity-based control of biped locomotion. IEEE Robot Autom Magaz 2007;14(2):30–40.
[29] Toibero JM, Soria C, Roberti F, Carelli R, Fiorini P. Switching visual servoing approach for stable corridor navigation. In: International conference on advanced robotics. Munich, Germany; 2009. p. 1–6.
[30] Van der Scaft A. L_2 gain and passivity techniques in nonlinear control. Verlag; 2000.
[31] Vidyasagar M. Nonlinear systems analysis. Prentice Hall International Editions; 1978.

[32] Vidyasagar M. New passivity-type criteria for large-scale interconnected systems. IEEE Trans Automat Control 1979;24:575–9.
[33] Weiss LE, Sanderson A, Neuman P. Dynamic sensor-based control of robots with visual feedback. IEEE J Robot Autom 1987;3(9):404–17.
[34] Zulli R, Fierro R, Conte G, Lewis FL. Motion planning and control for nonholonomic mobile robots. In: Proceedings of the IEEE international symposium on intelligent control; 1995. p. 551–7.